

Total and state-specific electron-ion recombination rates and photoionization of Ca XV for high temperature plasma

Sultana N. Nahar

Department of Astronomy, The Ohio State University, Columbus, OH 43210, USA

ARTICLE INFO

Keywords:

Photoionization
Electron-ion recombination
Ca XV
Unified method for recombination rates and spectrum
Total and state-specific rate coefficients
Excited states up to $n=10$
High temperature plasma
32.10-f
95.30.ky
32.80-t

ABSTRACT

The inverse processes of photoionization and electron-ion recombination of $(\text{Ca XV} + h\nu \leftrightarrow \text{Ca XVI} + e)$, are studied using the unified method of Nahar and Pradhan for a large number of bound states, 582 in total with $n \leq 10$ and $l \leq 9$, for their characteristic features particularly in the high energy region that can impact plasmas at high temperature. The unified method which implements close-coupling (CC) approximation and the R-matrix method includes both the radiative recombination (RR) and dielectronic recombination (DR) for the total recombination and yields self-consistent sets of results for both the inverse processes. The present study, carried out in large scale computations, employs a large CC wavefunction expansion of 29 LS states belonging to $n=2,3$ complexes of the core ion Ca XVI, and appeared to be the first detailed study for the electron-ion recombination of the ion. The present results include (i) state-specific photoionization cross sections ($\sigma_{PI}(nLS)$) leaving the core ion in the ground state, (ii) state-specific recombination rate coefficients ($\alpha_{RC}(nLS, T)$) that include both the RR and DR, (iii) total recombination rate coefficients (α_{RC}) with temperature that include contributions of infinite number of recombined states, and (iv) a spectrum of total electron-ion recombination cross sections and rates with respect to photoelectron energy. The study finds that the core ion excitations from the ground to high $n=3$ states have introduced Rydberg resonances which are stronger and Seaton resonances which are more enhanced in the high energy region of σ_{PI} compared to those introduced by excitations to the $n=2$ states. Such features have contributed to the shape of the temperature dependent state-specific $\alpha_{RC}(nLS, T)$, and have resulted in three DR bumps/ shoulders in the high temperature region of the total $\alpha_{RC}(T)$ where the third DR bump at temperature of ~ 4 MK has raised $\alpha_{RC}(T)$ at high T above all previous rates. The results are expected to be accurate within 10%–15% and provide more complete and precise spectral modelings for the high temperature plasmas where the highly charged Ca XV is more abundant.

1. introduction

Photoionization and electron-ion recombination are two most common processes in astrophysical plasmas. While photoionization occurs with a radiative source, recombination of an electron to an ion can occur everywhere with or without a radiative source. The resonances of these processes can appear in absorption and emission spectra respectively and can be used for plasma diagnostics of density and temperature. Photoionization resonances dissolve in high density and high temperature plasmas raising the continuum and shape of the continuum. Atomic parameters of the two processes are needed in determination of ionization fractions in photoionized plasmas such as stars, nebulae and in coronal plasmas where ionization is dominated by electron impact ionization. The equation of balance in photoionized plasma (e.g. Pradhan and Nahar (2011)) requires both photoionization cross sections and total recombination rate coefficients to give the

ionization fractions needed for various astrophysical models. For coronal plasmas, the equation of balance requires total recombination rate coefficients and the electron impact ionization coefficient (e.g. Pradhan and Nahar (2011)). Without proper inclusion of resonant features in photoionization and electron-ion recombination, the astrophysical applications are expected to have large uncertainties. Highly charged carbon like calcium ion, Ca XV, exists in high temperature plasmas, such as in solar flares and corona (e.g. Dere (1978), Bhatia and Mason (1986) and Laming and Drake (1999)), astronomical objects, such as, Bootis (e.g. Laming and Drake (1999)). Lines of Ca XV play important role for diagnostics and modeling for both astrophysical and laboratory plasmas.

Detailed photoionization with autoionizing resonances of Ca XV was first studied using the R-matrix method but with a smaller close coupling (CC) wave function expansion that included 8 states belonging

E-mail address: nahar.1@osu.edu.

URL: <https://www.astronomy.ohio-state.edu/nahar.1>.

<https://doi.org/10.1016/j.newast.2022.101925>

Received 2 February 2022; Received in revised form 16 August 2022; Accepted 22 August 2022

Available online 6 September 2022

1384-1076/© 2022 Elsevier B.V. All rights reserved.

to $n = 2$ complex of the core ion Ca XVI by Luo and Pradhan (1989), and later by Nahar and Pradhan (1992a) under the Opacity Project (Seaton, 1987; The Opacity Project Team, 1995). In a later study to observe the impact of high lying excitations of the core, Nahar (2017) used a larger wavefunction expansion of 29 states belonging to $n = 2,3$ complexes, and found dominant features in the high energy region of the total photoionization cross section of Ca XV arising from core ion excitation to $n = 3$ states. The present study implements the same wavefunction expansion for computing the partial photoionization cross sections for leaving the residual ion in the ground state. These cross sections are different from those obtained earlier for the total photoionization. Total photoionization cross sections consider all channels for excitations of the core ion to various states and cannot be used for electron-ion recombination of the core ion in the ground state.

Literature search shows limited study on the electron-ion recombination cross sections and rate coefficients for Ca XV and hence little data are available for modeling of astrophysical and laboratory plasmas. The earlier study of electron-ion recombination of Ca XV corresponds to obtaining radiative recombination (RR) rate coefficients through extrapolation of available rates for carbon sequence by Shull and Steenberg (Shull and Van Steenberg, 1982), and DR rates using isolated resonance approximation by Jacobs et al. (1980), Gu (2003) and Altun et al. (2004).

The present results provide the first detailed recombination rates for Ca XV. The present work, carried out under the Iron Project (IP) (Hummer et al., 1993), uses the unified method of Nahar and Pradhan (1992b, 1994) and Nahar (1996) for the total electron-ion recombination that implements ab initio close coupling approximation and the R-matrix method developed under the Opacity Project (OP) (The Opacity Project Team, 1995) and the IP (Hummer et al., 1993). One main objective of the present work is to study and obtain precise total recombination rates for high temperature plasmas, such as, coronal plasma.

2. Theory of photoionization and electron-ion recombination

The inverse processes of photoionization and electron-ion recombination can be direct as

$$h\nu + X^+ \rightleftharpoons e + X^{++}, \quad (1)$$

for which the electron-ion recombination is known as the radiative recombination (RR) that provides the background cross sections. However, when the energy of the photon matches to that of a quasi-bound quantum mechanical state, $(S_i L_i \pi_i) \nu l$ of the Rydberg series of states belonging to the excited core ion state $S_i L_i \pi_i$, lying above the ionization threshold, the inverse processes proceed via an intermediate doubly excited state known an autoionizing state, as

$$e + X^{++} \rightleftharpoons (X^+)^{**} \rightleftharpoons \begin{cases} (a) e + X^{++}(AI) \\ (b) h\nu + X^+(DR) \end{cases} \quad (2)$$

The outer electron is in the excited orbital νl where ν is the effective quantum number. An autoionizing state breaks either in to autoionization (AI) where the electron goes free or to dielectronic recombination (DR) where the electron is captured by emission of a photon (e.g. Pradhan and Nahar (2011)). This two-step process introduces a resonance both in photoionization and in electron-ion recombination. Resonances introduce various shapes and structures in the cross section of the process. Theoretically a resonance can be created naturally by including the core ion excitations in the wave function, as treated in close-coupling (CC) approximation.

The unified method for the total electron-ion recombination (Nahar and Pradhan, 1992b, 1994) implements the CC approximation and is an extension of the R-matrix method for atomic processes (e.g. Burke and Robb (1975), Scott and Burke (1980), Scott and Taylor (1982), Berrington et al. (1987, 1995) and Pradhan and Nahar (2011)) as developed under the OP and IP. In the CC approximation, the atomic

system is described as a core ion of N -electrons interacting with the $(N + 1)$ th electron. The total wave function, Ψ_E , in a symmetry $S L \pi$ is represented by the expansion

$$\Psi_E(e + ion) = A \sum_i \chi_i(ion) \theta_i + \sum_j c_j \Phi_j, \quad (3)$$

The first term on the right contains core ion eigenfunction, χ_i , coupled with the interacting $(N + 1)$ th electron function, θ_i , and the sum is over the ground and excited states of the core ion. The $(N + 1)$ th electron with kinetic energy k_i^2 is in a channel labeled as $S_i L_i \pi_i k_i^2 \ell_i (S L \pi)$. In the second sum, the Φ_j s are the bound channel functions of the $(N + 1)$ -electrons system that account for the short range correlation and the orthogonality between the continuum and the bound electron orbitals. Substitution of $\Psi_E(e + ion)$ expansion in the Schrodinger equation

$$H_{N+1} \Psi_E = E \Psi_E, \quad (4)$$

leads to a set of coupled equations that are solved using the R-matrix method (e.g. Burke and Robb (1975), Berrington et al. (1987, 1995) and Pradhan and Nahar (2011)). The $(N + 1)$ th electron is bound when the total energy is negative ($E < 0$), and the solution corresponds to a bound wavefunction, Ψ_B , and in the continuum when it is positive ($E > 0$) and the solution corresponds to a free or continuum wavefunction Ψ_F . The complex resonant structures in photoionization and recombination cross sections result from couplings between the continuum channels and bound channels in the transition matrix at electron energies k_i^2 corresponding to autoionizing states of the Rydberg series, $S_i L_i \pi_i \nu \ell$.

The present calculations have been carried out in LS coupling approximation where the Hamiltonian of the $(N + 1)$ -electrons has the kinetic and potential energy terms as

$$H_{N+1} = \sum_{i=1}^{N+1} \left\{ -\nabla_i^2 - \frac{2Z}{r_i} + \sum_{j>i}^{N+1} \frac{2}{r_{ij}} \right\}, \quad (5)$$

expressed in Rydberg unit system (e.g. Pradhan and Nahar (2011)). The Hamiltonian also includes relativistic mass correction and Darwin terms (e.g. Pradhan and Nahar (2011)).

Transition matrix elements for photoionization and electron-ion recombination, which require bound and continuum wavefunctions, can be expressed as $T_{BF} = \langle \Psi_B | \mathbf{D} | \Psi_F \rangle$ where $\mathbf{D} = \sum_i r_i$ is the dipole operator and the sum is over the number of electrons. The modulus squared of T_{BF} gives the generalized line strength as (e.g. Pradhan and Nahar (2011))

$$S = |\langle \Psi_f | \mathbf{D} | \Psi_i \rangle|^2 = \left| \left\langle \Psi_f \left| \sum_{j=1}^{N+1} r_j \right| \Psi_i \right\rangle \right|^2, \quad (6)$$

where Ψ_i and Ψ_f are the initial and final state wave functions. The photoionization cross section (σ_{PI}) is proportional to the generalized line strength (e.g. Pradhan and Nahar (2011)),

$$\sigma_{PI} = \frac{4\pi^2}{3c} \frac{1}{g_i} \omega S, \quad (7)$$

where g_i is the statistical weight factor of the bound state and ω is the incident photon energy. Recombination cross sections, σ_{RC} , can be obtained from detailed *partial* photoionization cross section using the principle of detailed balance as (e.g. Pradhan and Nahar (2011)),

$$\sigma_{RC} = \sigma_{PI} \frac{g_i}{g_j} \frac{h^2 \omega^2}{4\pi^2 m^2 c^2 v^2}. \quad (8)$$

where g_j is the statistical weight factor of the recombined state and v is the photoelectron velocity. The state-specific recombination rate coefficient of state i is obtained by averaging the recombination cross sections over Maxwellian distribution function $f(v)$ as

$$\alpha_R(i; T) = \int_0^\infty v f(v) \sigma_{RC}(i) dv, \quad f(v) = \frac{4}{\sqrt{\pi}} \left(\frac{m}{2kT} \right)^{3/2} v^2 e^{-\frac{mv^2}{2kT}} \quad (9)$$

The recombining ion is assumed to be in the ground state. The detailed autoionizing structures in σ_{PI} are integrated for σ_{RC} and hence

corresponds to inclusion of both the RR and DR in an unified and *ab initio* manner. The total recombination rate can be obtained from sum of these individual rates, that is, $\alpha_R(T) = \sum_i \alpha_R(i, T)$ where the sum is over infinite number of recombined states.

The unified method divides the infinite recombined states into two groups: group (A) states with $n \leq n_o$, and group (B) states with $n_o < n \leq \infty$, where $n_o \sim 10$. The recombination rates coefficients of group (A) states are obtained from detailed photoionization cross sections as described above. Recombination into group (B) states, which are in a small energy range, is dominated by DR via high-n resonances belonging to various excited core thresholds with small contributions of RR. The precise DR theory by Bell and Seaton (1985) was extended by Nahar and Pradhan (1992b, 1994) and Nahar (1996) to obtain the DR collision strengths, $\Omega(DR)$, as

$$\Omega(DR) = \sum_{SL\pi} \sum_n \frac{1}{2} (2S+1)(2L+1) P_n^{SL\pi}(DR). \quad (10)$$

where $P_n^{SL\pi}(DR) = (1 - S_{ee}^\dagger S_{ee})_n$ is the DR probability in entrance channel n . S_{ee} is the electron scattering matrix including radiation damping. $\Omega(DR)$ is obtained from the sum over all contributing symmetries $SL\pi$. Calculations for $\Omega(DR)$ are carried out in the CC approximation using the same wave function expansion used for photoionization cross sections and hence are self-consistent with σ_{PI} . The recombination cross section is then obtained as (e.g. Pradhan and Nahar (2011)),

$$\sigma_{RC}(DR) = \frac{\pi}{g_i k^2} \Omega(DR) a_o^2, \quad (11)$$

The RR ‘background’ contributions from the high-n group (B) states $n_o < n \leq \infty$, obtained in hydrogenic approximation (Nahar, 1996) are typically small except at very low temperatures where electron energies are not high enough for core excitations.

The spectrum of the total electron-ion recombination with respect to photoelectron energy is of considerable interest as it reveals resonant features and is observable experimentally. The unified total recombination rate coefficients with photoelectron energy, $\alpha_R(E)$, can be obtained as

$$\alpha_R(E) = v \sigma_{RC}(E), \quad (12)$$

where v is the photoelectron energy and $\sigma_{RC}(E)$ is the summed cross sections of all symmetries.

3. Computation

Computation for the partial photoionization cross sections leaving the core ion the ground state has been carried out in a similar way the total photoionization cross sections were obtained (Nahar, 2017). These cross sections are new as they have been computed separately.

The R-matrix computations is initiated with the input wave function expansion of the core ion, typically obtained from atomic structure calculations using program SUPERSTRUCTURE (Nahar et al., 2003; Eissner and Jones, 1974). The present work uses the 29-CC wave function expansion of Ca XV obtained by Nahar (2017) from optimization of a set of configurations in Thomas–Fermi–Dirac–Amaldi potential implemented in SUPERSTRUCTURE (SS). It contains 29 states of the core ion Ca XVI. The SS energies of the 29 states are given in column E_c of Table 1. Column E provides the energies used in the Hamiltonian matrix. Values of E are the same as E_c except that the observed energies, if available in the NIST table, have replaced the calculated energies. The comparison between the two columns show larger differences for the $n = 2$ states, but about 1% for higher states. The large differences are compensated or reduced during R-matrix calculations by including larger number of configurations. The R-matrix calculations can process much larger set of configurations compared to atomic structure codes.

The 29-CC wavefunction includes excitations of $n = 2, 3$ complexes (see Table 1) and 11 of these excited states are dipole allowed transition

Table 1

The 29 LS states and energies (E) of the core ion Ca XVI included in the wave function expansion of Ca XV. Column E_c represents the calculated values from program SS and E represents those used in the Hamiltonian where values of E_c have been replaced by the available observed energies. The last column provides the A-values for transitions from the ground state, $2s^2 2p^2 P^o$, to the 11 dipole allowed states of the set of 29 states.

	State		E_c	$E(\text{Ry})$	A-values (s^{-1})
1	$2s^2 2p$	$^2 P^o$		0.0	
2	$2s 2p^2$	$^4 P$	2.1611	2.63567	
3	$2s 2p^2$	$^2 D$	3.9755	4.38214	3.500E+09
4	$2s 2p^2$	$^2 S$	5.0983	5.39634	1.495E+10
5	$2s 2p^2$	$^2 P$	5.4197	5.84754	2.723E+10
6	$2p^3$	$^4 S^o$	6.9544	7.60781	
7	$2p^3$	$^2 D^o$	8.0242	8.59161	
8	$2p^3$	$^2 P^o$	9.0417	9.64959	
9	$2s^2 3s$	$^2 S$	39.815	39.8154	8.679E+11
10	$2s^2 3p$	$^2 P^o$	40.9909	40.9909	
11	$2s 2p 3s$	$^4 P^o$	42.1534	42.1537	
12	$2s^2 3d$	$^2 D$	42.1119	42.4942	5.459E+12
13	$2s 2p 3s$	$^2 P^o$	42.7540	42.7540	
14	$2s 2p 3p$	$^4 D$	43.2337	43.2337	
15	$2s 2p 3p$	$^4 S$	43.4265	43.4265	
16	$2s 2p 3p$	$^4 P$	43.6088	43.6088	
17	$2s 2p 3p$	$^2 P$	43.1878	43.6224	2.296E+12
18	$2s 2p 3p$	$^2 D$	43.7929	43.7929	2.686E+12
19	$2s 2p 3p$	$^2 S$	44.1497	44.1497	2.724E+12
20	$2s 2p 3d$	$^4 F^o$	44.1611	44.1611	
21	$2s 2p 3d$	$^2 D^o$	44.4578	44.4578	
22	$2s 2p 3s$	$^2 P^o$	44.4652	44.4652	
23	$2s 2p 3d$	$^4 D^o$	44.4125	45.0267	
24	$2s 2p 3d$	$^2 P^o$	45.1593	45.1593	
25	$2s 2p 3d$	$^4 P^o$	44.5108	45.2262	
26	$2s 2p 3p$	$^2 P$	45.5712	45.5712	7.060E+11
27	$2s 2p 3p$	$^2 D$	45.6114	45.6114	1.900E+11
28	$2s 2p 3d$	$^2 F^o$	45.0666	45.6779	
29	$2s 2p 3p$	$^2 S$	45.9174	45.9174	3.418E+11

from the ground state $2s^2 2p^2 P^o$. Unified method requires the transition probabilities (A-values) of the core ion ground state to these states for the recombination cross sections. The A-values are given in Table 1. They were obtained from code SUPERSTRUCTURE (Eissner and Jones, 1974; Nahar et al., 2003).

Photoionization cross section were computed with a finer energy mesh to resolve the resonances in detail, particularly in the energy region near the ionization threshold. For example, 4000 energy points were computed to resolve the near threshold region of 0.4 Ry of each state. The exponential factor in the electron-ion recombination rate integral provides higher multiplication factor in the low energy region. Hence higher resolution ensures obtaining accurate contribution to recombination. Quantum defect energy mesh can be used to approximately map the resonances. However, due to channel couplings the resonant structures will show overlapping effects. The present work computed σ_{PI} at 19,691 energy points from R-matrix codes for each state of Ca XV. Seaton’s fitting formula or Kramer’s fit is used to extrapolate them until infinity for computation of recombination rate coefficients. The cross section results were processed with code PRCLS (Nahar, 1996).

State-specific recombination rate coefficients for all bound states with $n \leq 10$ of group (A) are computed using the program RECOMB (Nahar and Pradhan, 1991) and are added together for the group (A) contributions to the total. Contributions from group (B) high-n states that lie below the target thresholds are obtained from the total DR collision strength $\Omega(DR)$ obtained using program STGFDR (Nahar and Pradhan, 1992b, 1994). The RR contribution (non-resonant) of the background from high-n states ($10 < n \leq \infty$) is included as the ‘‘top-up’’ part obtained in hydrogenic approximation (Nahar, 1996). The total unified recombination rate coefficients $\alpha_{RC}(T)$ with temperature, and those, $\alpha_{RC}(E)$ and the total recombination cross sections $\sigma_{RC}(E)$ with photoelectron energy E , were obtained by adding contributions from all states $n \leq \infty$ using program RECXS (e.g. Nahar et al. (2000)).

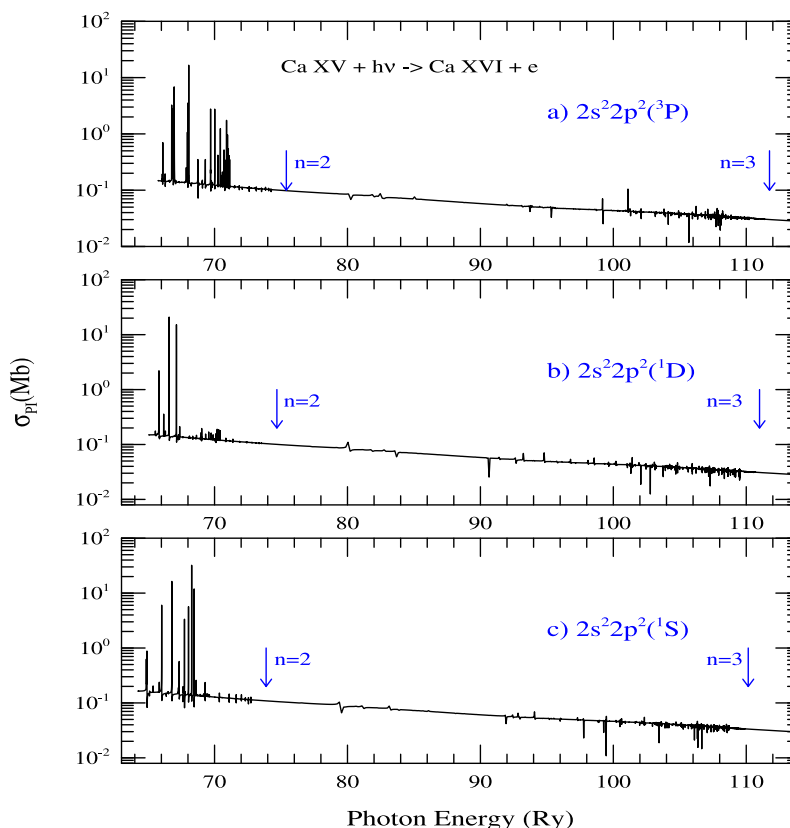


Fig. 1. Photoionization cross sections σ_{PI} of the three states of the ground configuration of Ca XV obtained from 29-CC calculations: (a) the ground $2s^2 2p^2(^3P)$ state, and excited (b) $2s^2 2p^2(^1D)$, (c) $2s^2 2p^2(^1S)$ states. They show that Rydberg resonances due to core ion excitations to $n = 2$ states (highest state pointed by arrow $n = 2$) are more visible than the much weaker resonances in the high energy region belonging to the excitations to $n = 3$ states. The background σ_{PI} decreases slowly with higher energy.

4. Results and discussions

The present work reports study of the two inverse processes of photoionization and electron-ion recombination of the ground and many excited states of Ca XV and illustrate their characteristic features that are inter-related to both the processes. Atomic states contribute differently to photoionization cross sections and electron-ion recombination rates because of the differences in energy positions of resonances and the shape and structure of the background cross section with energies. We find dominant features in the high energy region of most of the excited states which will impact the astrophysical modeling of the ion in high temperature plasmas.

We present state-specific photoionization cross sections (σ_{PI}) and electron-ion recombination cross sections (σ_{RC}) and rate coefficients ($\alpha_{RC}(nLS)$) for a total of 582 bound states with $n \leq 10$ and $l \leq 9$ of Ca XV. Only the singlet and triplet bound states are considered since for recombination the core ion (Ca XVI) ground state, $2s^2 2p(^2P^o)$, can couple to a partial wave to form only singlet and triplet states of Ca XV.

4.1. Photoionization cross sections

The earlier study on the total photoionization cross sections (Nahar, 2017) showed enhancement in the background and existence of strong high peak resonances in the high energy region introduced by the excitations to high lying states belonging to $n = 3$ complex in the core ion. The present study, which investigates the partial photoionization cross sections leaving the core ion in the ground state, also finds presence of high peak strong resonances in the high energy region. These features affect the state-specific and total recombination cross sections and rate coefficients. The present wavefunction includes all possible dipole allowed states of Ca XVI of configurations, $2s^2 2p$, $2s 2p^2$, $2p^3$, $2s^2 3s$, $2s^2 3p$, $2s^2 3d$, $2s 2p 3s$, $2s 2p 3p$, $2s 2p 3d$ of $n = 2, 3$ complexes,

that can produce prominent Rydberg series of resonances. The author's long time study finds that resonant contributions due to transitions $\Delta n = 1$ in the core ion to photoionization and electron-ion recombination are considerably more than those from $\Delta n = 0$ (e.g. Nahar (1995)) and the resonances diminish considerably beyond $\Delta n = 1$ transitions (e.g. Nahar (1998) and Nahar and Pradhan (2016)) indicating converging of resonances.

The features of photoionization can be generalized to form for four different types of states — the state or states of the ground configuration, excited equivalent electron states, low-lying excited single valence electron states and high lying excited single valence electron states. These features are described below with example states that contribute importantly to the electron-ion recombination of Ca XV.

The ground state often plays a most significant role because of its relatively higher background which decreases slowly with higher energy, as seen in Fig. 1 for Ca XV. The figure presents σ_{PI} of the three states of the ground configuration - (a) ground $2s^2 2p^2(^3P)$ state, and excited (b) $2s^2 2p^2(^1D)$, and (c) excited $2s^2 2p^2(^1S)$ states. The highest energy positions for the $n = 2$ and $n = 3$ states of the core ion are indicated by arrows. σ_{PI} of each state show visible resonances due to core excitations to $n = 2$ states, but very weak ones belonging to excitations to $n = 3$ states. These indicate no impact of $n = 3$ excitations or the large wavefunction expansion on the states of the ground configuration.

Photoionization cross sections of equivalent electron states, with two or more electrons in the outer orbital, of excited configurations also play dominant role in applications in general as these they have background cross section that varies slowly with higher energy. Ca XV has 9 excited states from equivalent electron configurations, $2s 2p^3$ ($^5S^o, ^3S^o, ^3D^o, ^1D^o, ^3P^o, ^1P^o$) and $2p^4$ ($^3P, ^1D, ^1S$). $^5S^o$ does not contribute to recombination as it cannot form from core ion ground state $2s^2 2p(^2P^o)$ in LS coupling. Fig. 2 presents features of two equivalent

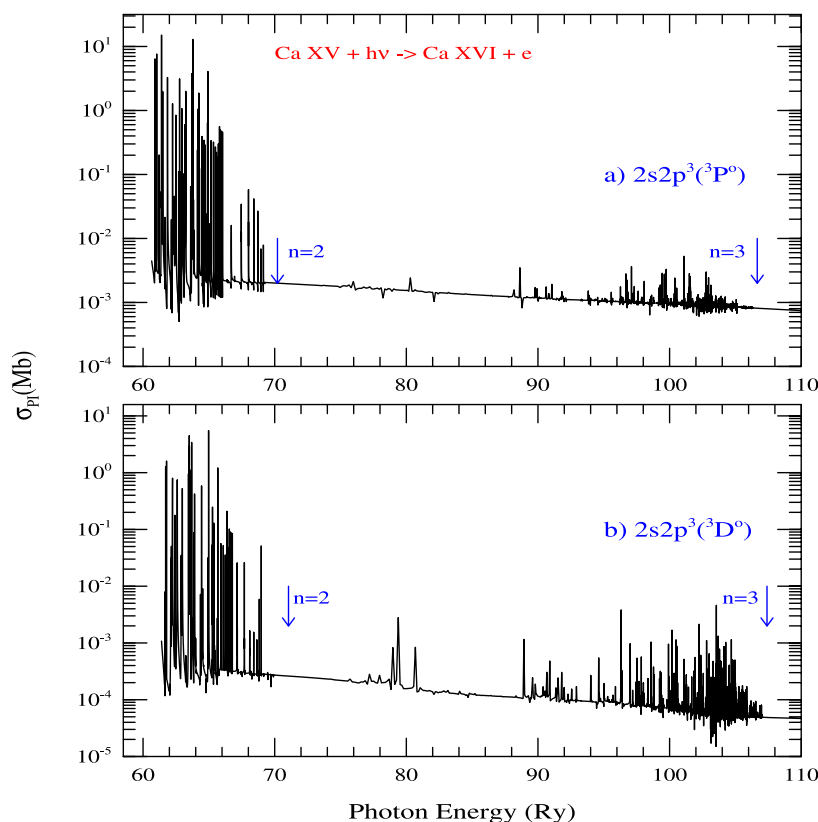


Fig. 2. σ_{PI} of two equivalent electron states of an excited configuration of Ca XV: (a) $2s2p^3(^3P^o)$ and (b) $2s2p^3(^3D^o)$. The arrows point the energy limits of the core excitations to $n = 2$ and 3 complexes. The background is decreasing slowly and the resonances due to core ion excitations to $n = 2$ states are prominent, and can be significant for $n = 3$ states, such as, for $2s2p^3(^3D^o)$ state.

electron states of Ca XV, (a) $2s2p^3(^3P^o)$ and (b) $2s2p^3(^3D^o)$ which show the slow decrease in the background with energy. However, unlike Fig. 1, these excited states, particularly $2s2p^3(^3D^o)$, have significant number of resonances belonging to core excitations to $n = 2$ states. For Ca XV, these states will contribute significantly in the low temperature plasmas due to their dense and high peak resonances in the energy region between the ionization threshold and core ion excitation to $n = 2$ states, and in the higher temperature region by the slow varying background cross section and high lying resonances.

For the excited single valence electron states, the core ion excitations to the high lying states have much more impact on photoionization than to the ground and equivalent electron states. They introduce strong high-peak Rydberg series of resonances in the high energy region and also contribute in the shape of the background. Fig. 3 illustrates features in σ_{PI} of two single valence electron excited states of Ca XV, (a) $2s^22p3p(^3D)$ and (b) $2s^2p3d(^3F^o)$. They are relatively low lying excited states of Ca XV. Both states show large differences in resonances belonging to core excitations to $n = 2$ and to $n = 3$ states. In each panel the low energy region of σ_{PI} has weak resonances belonging to $n = 2$ complex followed by a smooth background that is decreasing with energy until stronger resonances start to appear in the high energy region. With higher energy the excitations to $n = 3$ states have introduced very high peak strong Rydberg series of resonances that are much higher than those belonging to $n = 2$ states and the cross section at the ionization threshold. The red arrows in the figure shows energy positions of the excited core ion states where Rydberg series converge. Both of these states contribute significantly in the high temperature region of recombination rate coefficients α_{RC}

For the high-lying excited single valence electron states, the most prominent feature is the presence of Seaton resonances that often dominate the high energy region (Yu and Seaton, 1987; Pradhan and Nahar,

2011) and are important contributors to the electron-ion recombination in high temperature plasmas. A Seaton resonance is formed when the core ion absorbs the photon that matches the transition energy of the ground state to a dipole allowed excited state and the excitation leads to ionization as the core ion drops down to the ground state. The outer electron remains at its orbit when photo-excitation-of-core (PEC) takes place. In contrast to Rydberg resonances whose positions move with the ionization energy of the state, Seaton resonances appear at the fixed photon energies that equal to the transition energies of the core ion. A Seaton resonance is inverse to DR, and often manifests to a wider resonance with enhanced background in interference with the Rydberg resonances as shown in Fig. 4. Fig. 4 presents two highly excited states (a) $2s^22p5g(^3H^o)$ and (b) $2s^22p5f(^3F^o)$ of Ca XV that are dominant contributors in the high temperature recombination. The presence of broad and high peak Seaton resonances are pointed by arrows in the figure. They are showing prominence for $\Delta n = 2 - 3$ transitions. Seaton resonances due to $\Delta n = 2 - 2$ transitions are not visible in the figure as they lie below the ionization thresholds of the two states. Prominence of Seaton resonances can be explained by the transition probabilities (A-values) which give the measure of strength of excitation. The A-values in Table 1, which presents the 11 possible dipole allowed transitions in the set, show that A-values for $n = 2 - 2$ transitions are of order 10^{9-10} while $n = 2 - 3$ are of higher order 10^{11-12} . Seaton resonances become narrower and reduced peak for very high excited states.

4.2. State-specific recombination rate coefficients

State specific recombination rate coefficient, $\alpha_{RC}(nLS\pi)$, of each of the 582 bound states of Ca XV presented here represents approximately the total rate for the individual state since both the RR and DR are included in them by the unified method. The features of $\alpha_{RC}(nLS\pi)$

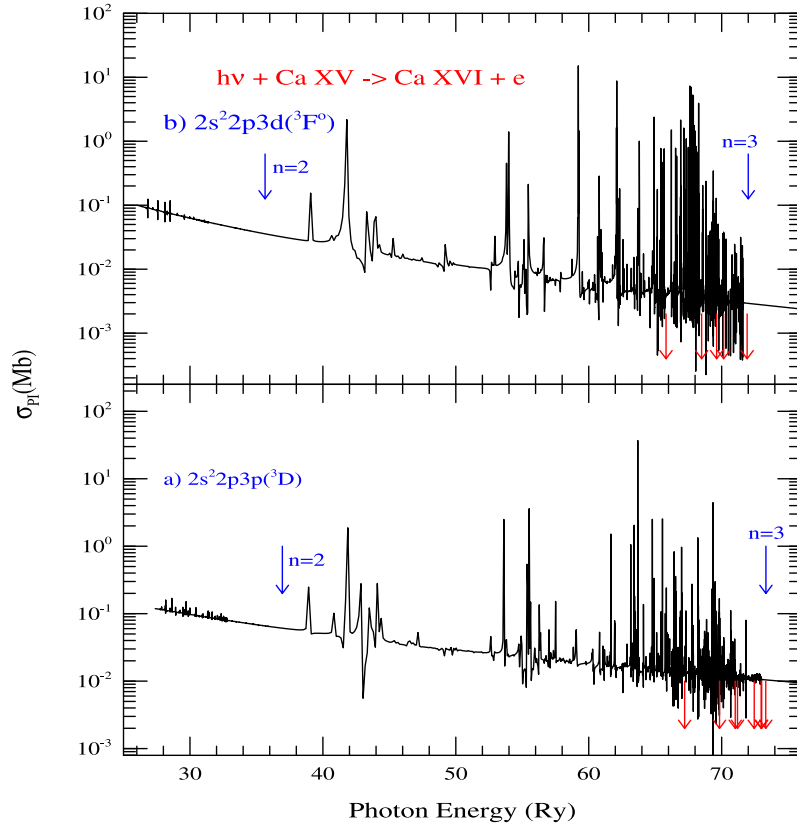


Fig. 3. σ_{PI} of two low lying single valence electron excited states of Ca XV from 29-CC calculations: (a) $2s^2 2p 3p(^3D)$, (b) $2s^2 2p 3d(^3F^0)$. Both states show weak resonances due to $n = 2$ excitations beyond which σ_{PI} decreases smoothly. However, strong and high-peak resonances appear due to core ion excitations to $n = 3$ states. They are denser and the peaks are much higher than those belonging to $n = 2$ excitations. The red arrows indicate energy positions of excited thresholds of the core ion, relative to the ionization threshold, to which Rydberg series of resonances converge. Arrows with $n = 2$ and $n = 3$ indicate limit to the highest core excitations of the complexes.

Table 2

List of 20 topmost states out of 582 of Ca XV and their state-specific recombination rate coefficients α_{RC} ($\text{cm}^3 \text{s}^{-1}$) in order of their contributions to the total α_{RC} at temperatures 1000, 10 000, 10^5 , and 10^6 K.

State T(K) = 10^3	α_{RC}	State 10^4	α_{RC}	State 10^5 K	α_{RC}	State 10^6	α_{RC}
$2s^2 2p^2 \ ^3 P^e$	3.95E-11	$2s^2 2p^2 \ ^3 P^e$	1.25E-11	$2s^2 2p^2 \ ^3 P^e$	5.17E-12	$2s^2 2p^2 \ ^3 P^e$	1.44E-12
$2s^2 2p^2 \ ^3 P^e$	3.95E-11	$2s^2 2p^2 \ ^3 P^e$	1.25E-11	$2s^2 2p^2 \ ^3 P^e$	5.17E-12	$2s^2 2p^2 \ ^3 P^e$	1.44E-12
$2s^2 2p^2 \ ^1 D^e$	2.18E-11	$2s^2 2p^2 \ ^1 D^e$	6.91E-12	$2s^2 2p^2 \ ^3 P^o$	4.23E-12	$2s^2 2p^2 \ P^o 3s^1 P^o$	8.37E-13
$2s^2 2p^2 \ P^o 3d^3 F^o$	9.83E-12	$2s^2 2p^2 \ P^o 3d^3 F^o$	3.10E-12	$2s^2 2p^2 \ ^1 P^o$	2.80E-12	$2s^2 2p^2 \ ^1 D^e$	7.96E-13
$2s^2 2p^2 \ P^o 3p^3 D^e$	9.19E-12	$2s^2 2p^2 \ P^o 3p^3 D^e$	2.91E-12	$2s^2 2p^2 \ ^1 D^e$	2.74E-12	$2s^2 2p^2 \ P^o 3d^1 D^o$	7.05E-13
$2s^2 2p^2 \ P^o 3d^3 D^o$	6.20E-12	$2s^2 2p^2 \ P^o 3d^3 D^o$	1.95E-12	$2s^2 p^2 S^e 3d^3 D^e$	1.97E-12	$2s^2 2p^2 \ P^o 3d^1 F^o$	6.68E-13
$2s^2 2p^2 \ P^o 4d^3 F^o$	5.50E-12	$2s^2 2p^2 \ P^o 4d^3 F^o$	1.73E-12	$2s^2 2p^2 \ ^1 D^o$	1.40E-12	$2s^2 2p^2 \ ^3 P^o$	4.63E-13
$2s^2 2p^2 \ P^o 3p^3 P^e$	5.03E-12	$2s^2 2p^2 \ P^o 3p^3 P^e$	1.59E-12	$2p^3 \ ^2 P^o 8 f^3 G^e$	1.20E-12	$2s^2 2p^2 \ P^o 3d^1 P^o$	3.87E-13
$2s^2 2p^2 \ ^1 S^e$	4.67E-12	$2s^2 2p^2 \ ^1 S^e$	1.48E-12	$2s^2 2p^2 \ ^3 D^o$	1.20E-12	$2s^2 2p^2 \ ^1 P^o$	3.84E-13
$2s^2 2p^2 \ P^o 3s^3 P^o$	4.55E-12	$2s^2 2p^2 \ P^o 3s^3 P^o$	1.45E-12	$2s^2 p^2 P^e 4d^3 P^e$	1.04E-12	$2s^2 2p^2 \ ^1 D^o$	3.49E-13
$2s^2 2p^2 \ P^o 3d^3 P^o$	4.09E-12	$2s^2 2p^2 \ P^o 3d^3 P^o$	1.29E-12	$2s^2 p^2 P^e 4s^3 P^e$	9.58E-13	$2s^2 2p^2 \ P^o 3p^3 D^e$	3.34E-13
$2s^2 2p^2 \ P^o 4p^3 D^e$	4.00E-12	$2s^2 2p^2 \ P^o 4p^3 D^e$	1.26E-12	$2s^2 2p^2 \ P^o 3d^3 F^o$	9.51E-13	$2s^2 2p^2 \ P^o 3p^3 P^e$	3.06E-13
$2s^2 2p^2 \ P^o 4d^3 D^o$	3.79E-12	$2s^2 2p^2 \ P^o 4d^3 D^o$	1.24E-12	$2s^2 2p^2 \ P^o 3p^3 D^e$	9.24E-13	$2s^2 2p^2 \ P^o 3d^3 F^o$	3.01E-13
$2s^2 2p^2 \ P^o 4f^3 G^e$	3.26E-12	$2s^2 2p^2 \ P^o 4d^3 D^o$	1.19E-12	$2s^2 p^2 D^e 4d^3 P^e$	8.14E-13	$2s^2 2p^2 \ P^o 3s^3 P^o$	2.75E-13
$2s^2 2p^2 \ P^o 5d^3 F^o$	3.20E-12	$2s^2 2p^2 \ P^o 4f^3 G^e$	1.02E-12	$2s^2 p^2 S^e 4d^3 D^e$	8.05E-13	$2s^2 2p^2 \ P^o 3d^3 D^o$	2.60E-13
$2s^2 2p^2 \ P^o 5f^3 G^e$	2.92E-12	$2s^2 2p^2 \ P^o 5d^3 F^o$	1.01E-12	$2s^2 p^2 S^e 3p^1 P^o$	7.70E-13	$2s^2 p^2 S^e 3d^3 D^e$	2.48E-13
$2s^2 2p^2 \ P^o 3p^1 D^e$	2.82E-12	$2s^2 2p^2 \ P^o 5f^3 G^e$	9.15E-13	$2s^2 2p^2 \ P^o 4p^3 P^e$	7.46E-13	$2s^2 2p^2 \ ^3 D^o$	2.32E-13
$2s^2 2p^2 \ P^o 4f^3 F^e$	2.69E-12	$2s^2 2p^2 \ P^o 3p^1 D^e$	8.91E-13	$2s^2 p^2 S^e 3d^1 D^e$	7.38E-13	$2p^4 \ ^3 P^e$	2.29E-13
$2s^2 2p^2 \ P^o 4p^3 P^e$	2.42E-12	$2s^2 2p^2 \ P^o 4f^3 F^e$	8.41E-13	$2p^4 \ ^3 P^e$	6.79E-13	$2s^2 2p^2 \ P^o 3p^1 D^e$	1.74E-13
$2s^2 2p^2 \ P^o 3d^1 D^o$	2.42E-12	$2s^2 2p^2 \ P^o 4p^3 P^e$	8.00E-13	$2s^2 p^2 S^e 3p^3 P^o$	6.52E-13	$2s^2 p^2 D^e 3d^3 F^e$	1.69E-13
$2s^2 2p^2 \ P^o 4d^3 P^o$	2.35E-12	$2s^2 2p^2 \ P^o 3d^1 D^o$	7.60E-13	$2s^2 2p^2 \ P^o 3p^3 P^e$	6.29E-13	$2s^2 2p^2 \ ^3 S^o$	1.61E-13
Sum =	1.40E-10		4.49E-11		3.04E-11		8.72E-12
Total =	7.35E-10		1.84E-10		8.63E-11		4.68E-11
%contribution =	19%		24%		35%		19%

depend on the resonant positions and structures and background cross section of photoionization. Table 2 list top 20 states of Ca XV in order of their' contributions to the total recombination rate coefficient α_{RC} at four different temperatures. It can be seen that at each temperature,

the set of dominant states is different and their order of contribution to the total rate is different. The reason is that contributions of the states are dependent on the energy positions and strengths of the resonances in photoionization cross sections of the state.

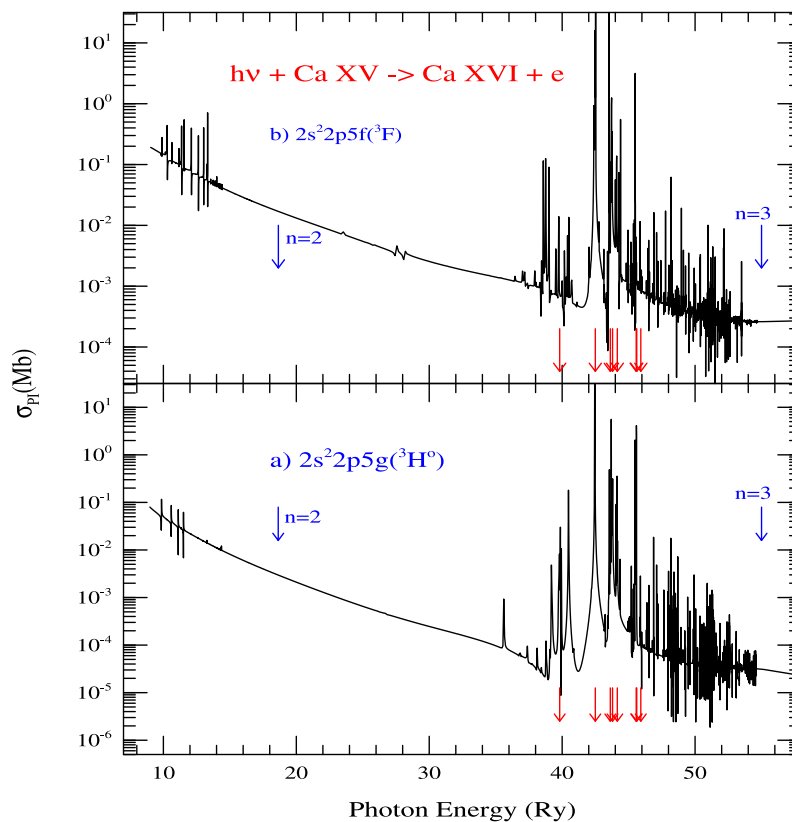


Fig. 4. σ_{pi} of two highly excited states of Ca XV illustrating Seaton resonances due to PEC: (a) $2s^2 2p 5g(^3H^o)$, (b) $2s^2 2p 5f(^3F^o)$. The states show wide and high peak Seaton resonances (positions are marked by arrows) enhancing the background considerably. Blue arrows point to the energy limits with core excitations to $n = 2$ and 3 complexes.

Fig. 5 presents temperature dependent features of state-specific recombination rate coefficients $\alpha_{RC}(nLS, T)$ of 7 states selected from Table 2, (a) the ground state $2s^2 2p^2(^1D)$, and a number of excited states, (b) $2s^2 2p^2(^3D)$, (c) $2s^2 2p 3d(^3F^o)$, (d) $2s^2 2p 3p(^3D)$, (e) $2s^2 2p 3d(^3D^o)$, (f) $2s^2 2p 5f(^3F^o)$, (g) $2s^2 2p 5g(^3H)$ as illustrative examples. These states have been found to contribute significantly either in the low or in the high temperature regions of α_{RC} . $\alpha_{RC}(nLS, T)$ of the ground and equivalent electron states (panels a,b) show almost no feature while low lying single electron valence states (panels c,d,e) have a mild shoulder beyond 1 MK, and high lying excited states (panels f,g) have a visible and large DR bump at high temperature. The rise and formation of a bump or shoulder in α_{RC} in the high temperature region, also known as the DR bump, is mainly due to the presence of high peak Rydberg and wide Seaton resonances belonging to $n = 3$ excitations of the core ion in the high energy region. It is often assumed that the ground state of an ion contribute the most to electron-ion recombination. However, as these plots demonstrate, the contribution of an excited state may exceed to that of the ground state depending on the temperature region.

While all state-specific rate coefficients are available online, Table 3 presents $\alpha_{RC}(nLS, T)$ of 10 states of Ca XV that contribute dominantly in the temperature range of $10 - 10^9$ K, as needed for population modeling. The present state specific rates should be accurate for most of the temperature range except at lower temperature where uncertainty may be introduced even from slight shift or resonance positions. The resolution and precise positions of resonances become less significant at higher temperature as they are damped out by the exponential factor in the $\alpha_{RC}(nLS)$ integral.

4.3. Total recombination rate coefficients

The unified total recombination rate coefficients, $\alpha_R(T)$, of Ca XV are the added contributions of (a) the state-specific rate coefficients

$\alpha_{RC}(nLS, T)$ of 582 bound states with $n \leq 10$, (b) DR rates obtained using the extension of Nahar and Pradhan (1994) of the precise theory of Bell and Seaton theory (Bell and Seaton, 1985) and RR rates obtained in hydrogenic approximation as described in the unified method (Nahar and Pradhan, 1994; Nahar, 1996) of states with $10 < n \leq \infty$.

Features of the total $\alpha_R(T)$ with temperature are illustrated in Fig. 6, and are presented numerically in Table 4. Fig. 6 shows that total $\alpha_R(T)$ (red solid curve) starts with a high recombination rate at very low temperature where RR dominates, decreases smoothly with increasing temperature until it rises again. For Ca XV, $\alpha_R(T)$ starts forming, beyond 10,000 K, mild humps, 3 in total, around temperatures 1×10^5 , 4×10^5 , and 4×10^6 K respectively. In this temperature range, doubly excited states start to form leading the recombination through DR. The interference between RR and DR, which is important in this temperature range, shapes the curve for the total $\alpha_R(T)$ and unified method reproduces it naturally. So it removes the uncertainty introduced by adding RR and DR rates computed separately using different approximations. For example, sum of RR rates by Shull and Van Steenberg (1982) and DR rates by Jacobs et al. (1980), compared in the figure, will not consider the interference effect and may not produce the proper shape of the $\alpha_R(T)$. The multiple bumps indicate presence of strong resonances in photoionization cross sections at high energy formed by various core ion excitations. At even higher temperature, the exponential factor in the recombination rate coefficient integral dampens the DR contributions and $\alpha_R(T)$ decreases smoothly with temperature. The humps particularly the last one, at a temperature of solar corona where Ca XV is found to exist, has enhanced the recombination considerably. The figure presents other existing rates, such as, the RR rates (magenta dash) obtained by Shull and Van Steenberg (1982) through extrapolation of values of other isoelectronic ions, and DR rate coefficients obtained by Jacobs et al. (1980) (blue dot), Gu (2003) (black dot), Altun et al. (2004) (black dash), all using distorted wave approximation in the isolated resonance approximation. Altun et al. and Gu included

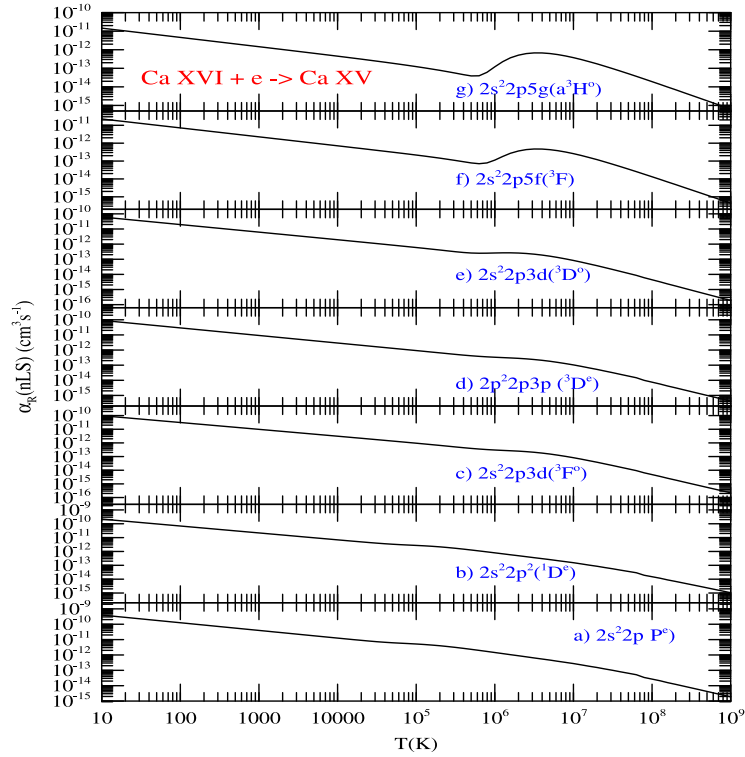


Fig. 5. State-specific recombination rate coefficients ($\alpha_{RC}(nSL\pi)$) of seven states, (a) $2s^2 2p^2(^3P)$, (b) $2s^2 2p^2(^1D)$, (c) $2s^2 2p 3d(^3F^o)$, (d) $2s^2 2p 3p(^3D)$, (e) $2s^2 2p 3d(^3D^o)$, (f) $2s^2 2p 5f(^3F)$, (g) $2s^2 2p 5g(^3H^o)$, of Ca XV that dominate low or high or both temperature regions. The features are introduced by the strength and energy positions of the resonant structures in σ_{PI} .

Table 3

Unified state-specific recombination rate coefficients ($\alpha_{RC}(SL\pi)$) of ten states of Ca XV that dominate the recombination at various temperatures. The number below each state is the binding energy (B.E.) in Ry of the state.

States:	logT (K)	$\alpha_{RC}(SL\pi)$ (cm^{-1})								
	1Po 1	1De 1	1Do 1	3Pe 1	3Po 1	3De 1	3Do 2	3Fe 8	3Fo 1	3Ho 2
B.E.	-58.5	-65.0	-59.3	-65.8	-60.7	-27.4	-25.7	-9.05	-26.0	-8.99
1.0	2.68E-12	2.18E-10	2.22E-12	3.96E-10	1.02E-11	9.20E-11	6.21E-11	2.26E-11	9.85E-11	1.46E-11
1.1	2.39E-12	1.94E-10	1.98E-12	3.53E-10	9.05E-12	8.19E-11	5.53E-11	2.02E-11	8.77E-11	1.30E-11
1.2	2.13E-12	1.73E-10	1.76E-12	3.14E-10	8.06E-12	7.30E-11	4.93E-11	1.80E-11	7.82E-11	1.16E-11
1.3	1.90E-12	1.54E-10	1.57E-12	2.80E-10	7.18E-12	6.51E-11	4.39E-11	1.60E-11	6.97E-11	1.04E-11
1.4	1.69E-12	1.37E-10	1.40E-12	2.50E-10	6.40E-12	5.80E-11	3.92E-11	1.43E-11	6.21E-11	9.22E-12
1.5	1.51E-12	1.22E-10	1.25E-12	2.22E-10	5.70E-12	5.17E-11	3.49E-11	1.27E-11	5.53E-11	8.22E-12
1.6	1.34E-12	1.09E-10	1.11E-12	1.98E-10	5.08E-12	4.61E-11	3.11E-11	1.13E-11	4.93E-11	7.33E-12
1.7	1.20E-12	9.72E-11	9.89E-13	1.77E-10	4.53E-12	4.10E-11	2.77E-11	1.01E-11	4.40E-11	6.53E-12
1.8	1.07E-12	8.66E-11	8.81E-13	1.57E-10	4.03E-12	3.66E-11	2.47E-11	9.01E-12	3.92E-11	5.82E-12
1.9	9.50E-13	7.72E-11	7.85E-13	1.40E-10	3.59E-12	3.26E-11	2.20E-11	8.03E-12	3.49E-11	5.19E-12
2.0	8.46E-13	6.88E-11	6.99E-13	1.25E-10	3.20E-12	2.91E-11	1.96E-11	7.15E-12	3.11E-11	4.62E-12
2.1	7.54E-13	6.13E-11	6.23E-13	1.11E-10	2.85E-12	2.59E-11	1.75E-11	6.37E-12	2.77E-11	4.12E-12
2.2	6.72E-13	5.47E-11	5.54E-13	9.93E-11	2.54E-12	2.31E-11	1.56E-11	5.68E-12	2.47E-11	3.67E-12
2.3	5.98E-13	4.87E-11	4.93E-13	8.85E-11	2.26E-12	2.06E-11	1.39E-11	5.06E-12	2.20E-11	3.27E-12
2.4	5.33E-13	4.34E-11	4.39E-13	7.89E-11	2.01E-12	1.83E-11	1.24E-11	4.51E-12	1.96E-11	2.91E-12
2.5	4.75E-13	3.87E-11	3.90E-13	7.03E-11	1.79E-12	1.63E-11	1.10E-11	4.02E-12	1.75E-11	2.60E-12
2.6	4.23E-13	3.45E-11	3.47E-13	6.27E-11	1.59E-12	1.46E-11	9.83E-12	3.58E-12	1.56E-11	2.31E-12
2.7	3.76E-13	3.08E-11	3.08E-13	5.58E-11	1.42E-12	1.30E-11	8.76E-12	3.19E-12	1.39E-11	2.06E-12
2.8	3.35E-13	2.74E-11	2.74E-13	4.98E-11	1.26E-12	1.16E-11	7.81E-12	2.85E-12	1.24E-11	1.84E-12
2.9	2.98E-13	2.44E-11	2.43E-13	4.44E-11	1.12E-12	1.03E-11	6.96E-12	2.54E-12	1.10E-11	1.64E-12
3.0	2.65E-13	2.18E-11	2.15E-13	3.95E-11	9.92E-13	9.19E-12	6.20E-12	2.26E-12	9.83E-12	1.46E-12
3.1	2.35E-13	1.94E-11	1.90E-13	3.52E-11	8.79E-13	8.19E-12	5.53E-12	2.02E-12	8.76E-12	1.30E-12
3.2	2.09E-13	1.73E-11	1.68E-13	3.14E-11	7.78E-13	7.30E-12	4.93E-12	1.80E-12	7.81E-12	1.16E-12
3.3	1.85E-13	1.54E-11	1.48E-13	2.80E-11	6.87E-13	6.51E-12	4.39E-12	1.60E-12	6.96E-12	1.03E-12
3.4	1.64E-13	1.37E-11	1.29E-13	2.50E-11	6.06E-13	5.80E-12	3.91E-12	1.43E-12	6.20E-12	9.16E-13
3.5	1.45E-13	1.23E-11	1.13E-13	2.22E-11	5.33E-13	5.17E-12	3.48E-12	1.27E-12	5.52E-12	8.15E-13
3.6	1.29E-13	1.09E-11	9.87E-14	1.98E-11	4.73E-13	4.61E-12	3.10E-12	1.13E-12	4.92E-12	7.25E-13
3.7	1.20E-13	9.74E-12	8.56E-14	1.77E-11	4.48E-13	4.11E-12	2.76E-12	1.01E-12	4.38E-12	6.44E-13
3.8	1.27E-13	8.68E-12	7.41E-14	1.57E-11	5.11E-13	3.66E-12	2.46E-12	8.99E-13	3.90E-12	5.72E-13
3.9	1.64E-13	7.74E-12	6.40E-14	1.40E-11	7.51E-13	3.26E-12	2.19E-12	8.00E-13	3.48E-12	5.08E-13
4.0	2.38E-13	6.91E-12	5.53E-14	1.25E-11	1.24E-12	2.91E-12	1.95E-12	7.13E-13	3.10E-12	4.51E-13

(continued on next page)

Table 3 (continued).

States:	logT (K)		$\alpha_{RC}(SL\pi)$ (cm ⁻¹)							
	1Po 1	1De 1	1Do 1	3Pe 1	3Po 1	3De 1	3Do 2	3Fe 8	3Fo 1	3Ho 2
4.1	3.46E-13	6.16E-12	4.81E-14	1.12E-11	1.95E-12	2.59E-12	1.74E-12	6.35E-13	2.76E-12	3.99E-13
4.2	4.90E-13	5.50E-12	4.32E-14	1.00E-11	2.79E-12	2.31E-12	1.55E-12	5.65E-13	2.45E-12	3.53E-13
4.3	7.00E-13	4.92E-12	4.53E-14	8.96E-12	3.63E-12	2.06E-12	1.37E-12	5.02E-13	2.18E-12	3.12E-13
4.4	1.02E-12	4.41E-12	7.00E-14	8.06E-12	4.35E-12	1.84E-12	1.22E-12	4.47E-13	1.94E-12	2.76E-13
4.5	1.46E-12	3.98E-12	1.47E-13	7.30E-12	4.89E-12	1.64E-12	1.09E-12	3.97E-13	1.73E-12	2.43E-13
4.6	1.96E-12	3.62E-12	3.10E-13	6.69E-12	5.20E-12	1.46E-12	9.64E-13	3.53E-13	1.53E-12	2.13E-13
4.7	2.41E-12	3.33E-12	5.63E-13	6.22E-12	5.26E-12	1.30E-12	8.56E-13	3.13E-13	1.36E-12	1.87E-13
4.8	2.73E-12	3.09E-12	8.73E-13	5.84E-12	5.09E-12	1.16E-12	7.60E-13	2.78E-13	1.21E-12	1.63E-13
4.9	2.85E-12	2.90E-12	1.17E-12	5.51E-12	4.73E-12	1.04E-12	6.74E-13	2.46E-13	1.07E-12	1.42E-13
5.0	2.80E-12	2.73E-12	1.40E-12	5.17E-12	4.23E-12	9.24E-13	5.96E-13	2.17E-13	9.51E-13	1.23E-13
5.1	2.60E-12	2.56E-12	1.52E-12	4.81E-12	3.68E-12	8.23E-13	5.27E-13	1.91E-13	8.42E-13	1.06E-13
5.2	2.32E-12	2.37E-12	1.53E-12	4.41E-12	3.12E-12	7.32E-13	4.65E-13	1.67E-13	7.43E-13	9.13E-14
5.3	2.00E-12	2.15E-12	1.44E-12	3.98E-12	2.60E-12	6.51E-13	4.09E-13	1.45E-13	6.55E-13	7.77E-14
5.4	1.67E-12	1.93E-12	1.29E-12	3.54E-12	2.12E-12	5.79E-13	3.58E-13	1.26E-13	5.76E-13	6.57E-14
5.5	1.37E-12	1.70E-12	1.11E-12	3.11E-12	1.70E-12	5.16E-13	3.15E-13	1.08E-13	5.06E-13	5.50E-14
5.6	1.10E-12	1.48E-12	9.28E-13	2.70E-12	1.35E-12	4.62E-13	2.80E-13	9.20E-14	4.46E-13	4.57E-14
5.7	8.62E-13	1.27E-12	7.50E-13	2.32E-12	1.05E-12	4.18E-13	2.58E-13	7.86E-14	3.95E-13	3.89E-14
5.8	6.67E-13	1.09E-12	5.92E-13	1.99E-12	8.09E-13	3.83E-13	2.50E-13	7.11E-14	3.55E-13	3.55E-14
5.9	5.09E-13	9.34E-13	4.58E-13	1.70E-12	6.15E-13	3.56E-13	2.52E-13	7.85E-14	3.25E-13	6.07E-14
6.0	3.84E-13	7.96E-13	3.49E-13	1.44E-12	4.63E-13	3.34E-13	2.60E-13	1.13E-13	3.01E-13	1.20E-13
6.1	2.86E-13	6.78E-13	2.62E-13	1.23E-12	3.46E-13	3.17E-13	2.66E-13	1.81E-13	2.83E-13	2.28E-13
6.2	2.12E-13	5.77E-13	1.95E-13	1.04E-12	2.57E-13	3.00E-13	2.66E-13	2.73E-13	2.67E-13	3.69E-13
6.3	1.56E-13	4.92E-13	1.43E-13	8.88E-13	1.90E-13	2.83E-13	2.58E-13	3.66E-13	2.49E-13	5.11E-13
6.4	1.14E-13	4.20E-13	1.05E-13	7.57E-13	1.40E-13	2.62E-13	2.41E-13	4.38E-13	2.30E-13	6.20E-13
6.5	8.33E-14	3.56E-13	7.62E-14	6.41E-13	1.03E-13	2.37E-13	2.17E-13	4.72E-13	2.06E-13	6.75E-13
6.6	6.06E-14	3.04E-13	5.51E-14	5.46E-13	7.60E-14	2.10E-13	1.89E-13	4.69E-13	1.80E-13	6.73E-13
6.7	4.41E-14	2.59E-13	3.98E-14	4.65E-13	5.61E-14	1.82E-13	1.60E-13	4.34E-13	1.53E-13	6.25E-13
6.8	3.20E-14	2.17E-13	2.86E-14	3.89E-13	4.14E-14	1.53E-13	1.31E-13	3.81E-13	1.27E-13	5.50E-13
6.9	2.33E-14	1.83E-13	2.05E-14	3.28E-13	3.08E-14	1.27E-13	1.06E-13	3.20E-13	1.03E-13	4.62E-13
7.0	1.69E-14	1.54E-13	1.47E-14	2.76E-13	2.29E-14	1.04E-13	8.33E-14	2.60E-13	8.25E-14	3.75E-13
7.1	1.23E-14	1.27E-13	1.05E-14	2.27E-13	1.70E-14	8.34E-14	6.45E-14	2.05E-13	6.45E-14	2.96E-13
7.2	8.93E-15	1.04E-13	7.51E-15	1.85E-13	1.27E-14	6.61E-14	4.93E-14	1.58E-13	4.99E-14	2.28E-13
7.3	6.51E-15	8.54E-14	5.37E-15	1.53E-13	9.50E-15	5.23E-14	3.74E-14	1.20E-13	3.83E-14	1.73E-13
7.4	4.74E-15	6.89E-14	3.83E-15	1.23E-13	7.09E-15	4.07E-14	2.81E-14	8.96E-14	2.91E-14	1.30E-13
7.5	3.47E-15	5.61E-14	2.74E-15	1.00E-13	5.34E-15	3.19E-14	2.11E-14	6.63E-14	2.20E-14	9.58E-14
7.6	2.53E-15	4.48E-14	1.95E-15	7.99E-14	4.00E-15	2.45E-14	1.56E-14	4.86E-14	1.65E-14	7.02E-14
7.7	1.86E-15	3.61E-14	1.40E-15	6.45E-14	3.02E-15	1.90E-14	1.16E-14	3.54E-14	1.24E-14	5.10E-14
7.8	1.37E-15	2.91E-14	9.97E-16	5.19E-14	2.29E-15	1.47E-14	8.62E-15	2.56E-14	9.34E-15	3.69E-14
7.9	9.45E-16	1.92E-14	7.03E-16	3.42E-14	1.56E-15	9.91E-15	6.01E-15	1.84E-14	6.45E-15	2.66E-14
8.0	6.91E-16	1.50E-14	5.02E-16	2.69E-14	1.17E-15	7.53E-15	4.41E-15	1.32E-14	4.78E-15	1.91E-14
8.1	5.05E-16	1.18E-14	3.58E-16	2.10E-14	8.73E-16	5.70E-15	3.23E-15	9.47E-15	3.53E-15	1.37E-14
8.2	3.64E-16	8.84E-15	2.55E-16	1.58E-14	6.40E-16	4.20E-15	2.33E-15	6.76E-15	2.57E-15	9.76E-15
8.3	2.66E-16	6.83E-15	1.82E-16	1.22E-14	4.77E-16	3.16E-15	1.70E-15	4.82E-15	1.89E-15	6.96E-15
8.4	1.94E-16	5.26E-15	1.30E-16	9.39E-15	3.56E-16	2.37E-15	1.24E-15	3.44E-15	1.39E-15	4.95E-15
8.5	1.42E-16	4.04E-15	9.25E-17	7.21E-15	2.65E-16	1.78E-15	9.06E-16	2.44E-15	1.02E-15	3.52E-15
8.6	1.04E-16	3.09E-15	6.60E-17	5.52E-15	1.98E-16	1.33E-15	6.61E-16	1.74E-15	7.53E-16	2.50E-15
8.7	7.61E-17	2.36E-15	4.72E-17	4.22E-15	1.48E-16	1.00E-15	4.82E-16	1.23E-15	5.54E-16	1.78E-15
8.8	5.58E-17	1.81E-15	3.37E-17	3.23E-15	1.10E-16	7.51E-16	3.52E-16	8.76E-16	4.09E-16	1.26E-15
8.9	4.09E-17	1.38E-15	2.41E-17	2.47E-15	8.23E-17	5.64E-16	2.58E-16	6.22E-16	3.01E-16	8.94E-16
9.0	3.01E-17	1.05E-15	1.72E-17	1.88E-15	6.15E-17	4.24E-16	1.89E-16	4.41E-16	2.23E-16	6.34E-16

contributions from radiative decay rates of transitions $\Delta n = 0, 1$. Gu provides separate fitting parameters for $\Delta n = 0$ and 1 (available from him) respectively which are added for the total DR rates. Both Gu and Altun et al. agree with each other at all temperature except for the low temperature rise. DR rates from both works are about 30% higher than the total unified rates in the temperature region where RR and DR interference is important. At very high temperature their rates are about the same as those of from the unified method. Comparison is also made with rates obtained using a 8-CC wavefunction expansion that considers excitations to $n = 2$ states but not $n = 3$ states of the core ion (Nahar, unpublished) and hence miss the enhancement from resonances due to core ion excitations to $n = 3$ states. It may be noted that although the individual states show different features, the summed rates statistically averaged them out and forms a general pattern.

4.4. Recombination spectrum

The total recombination rate coefficient with respect to photoelectron energy, $\alpha_R(E) = \sigma_{RC} \times v$ where v is the velocity of the electron and σ_{RC} is the total recombination cross section, reveals detailed features

and can be observed experimentally. Fig. 7 presents spectrum of total (a) σ_{RC} and (b) $\alpha_R(E)$ with electron energy of (e + Ca XVI \rightarrow Ca XV). The resonant structures at low energy are formed by the resonances in photoionization produced by excitations in $n = 2$ complex (pointed by arrows). The middle section resonances have been formed by the Seaton resonances and the third large broader set of structures have been formed by core ion excitations to $n = 3$ states. The arrows in Fig. 7 point positions of the core ion thresholds where resonances converged forming DR peaks. Recombination spectrum predicts high recombination rates in the photoelectron energy ranges of 1–80 eV, 180–260 eV, and of 350–600 eV.

5. Conclusion

The study presents photoionization cross sections and state-specific recombination rate coefficients of 582 bound states of Ca XV with the new features in the high energy region. Existence of extensive strong resonances and enhanced background cross sections are found to form due to core excitations to $n = 3$ complex. In addition Seaton resonances

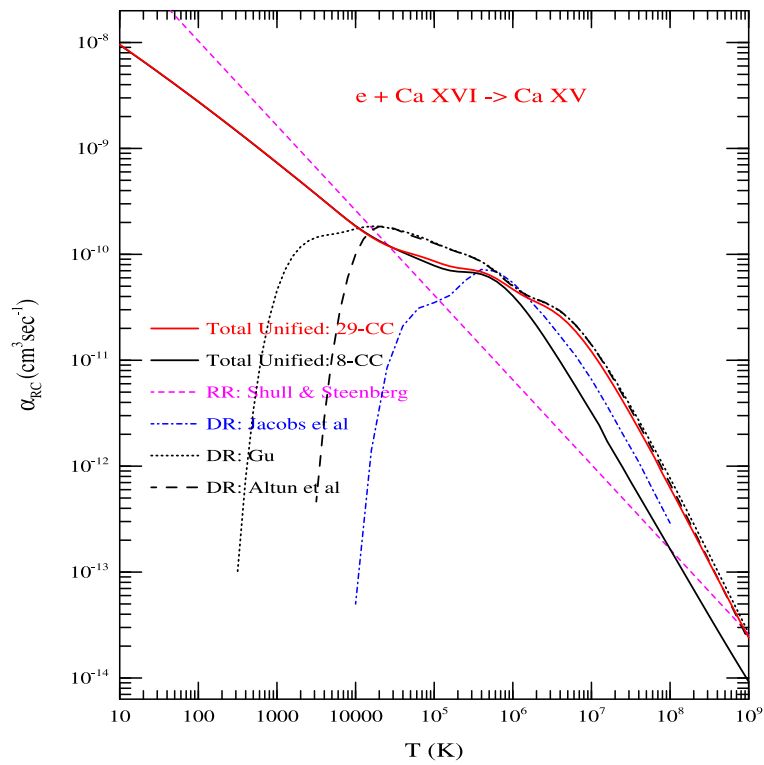


Fig. 6. Unified total recombination rate coefficients ($\alpha_{RC}(T)$) (solid red and black curves) of Ca XV with temperature. The features show presence of three humps on the rate, from 29-CC calculations, enhancing the recombination at high temperature (red), in comparison to 8-CC calculations (black) that did not include the resonances due to core ion excitations to $n = 3$ states. They are compared with existing RR rates obtained through extrapolation by Shull and Van Steenberg (1982), DR rates by Jacobs et al. (1980), Gu (2003), and Altun et al. (2004).

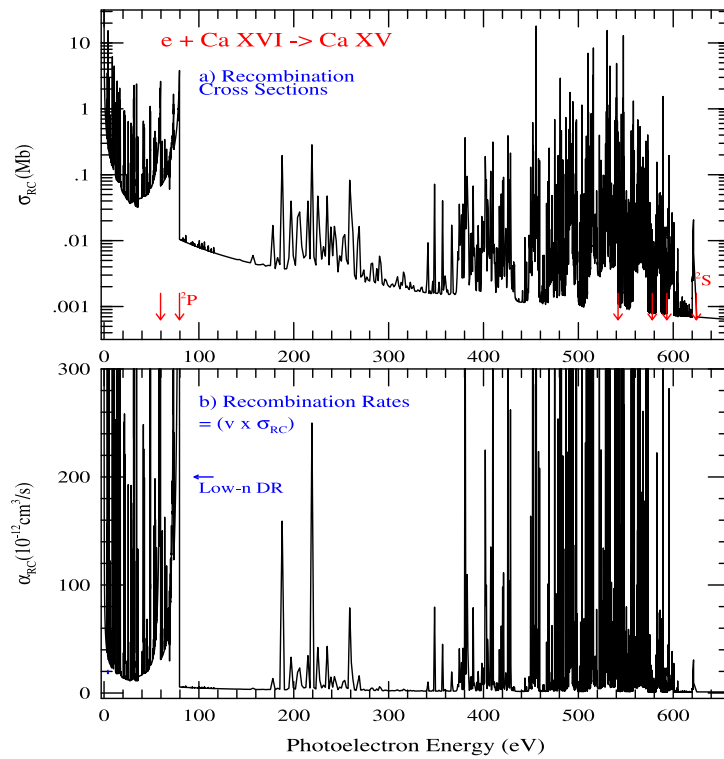


Fig. 7. Total unified recombination (a) cross section, σ_{RC} and (b) rate coefficient, α_{RC} , of Ca XV with respect to photo-electron energy in eV. The dominant resonant structures are in the photoelectron energy ranges of 1–80 eV, 180–260 eV and 350–600 eV.

Table 4
The total recombination rate coefficients ($\alpha_{RC}(T)$) of Ca XV with temperature.

logT (K)	$\alpha_{RC}(\text{cm}^3/\text{s})$	logT (K)	$\alpha_{RC}(\text{cm}^3/\text{s})$
1.0	9.555E-09	5.1	8.116E-11
1.1	8.471E-09	5.2	7.712E-11
1.2	7.507E-09	5.3	7.450E-11
1.3	6.653E-09	5.4	7.284E-11
1.4	5.887E-09	5.5	7.107E-11
1.5	5.200E-09	5.6	6.825E-11
1.6	4.593E-09	5.7	6.397E-11
1.7	4.056E-09	5.8	5.846E-11
1.8	3.572E-09	5.9	5.246E-11
1.9	3.146E-09	6.0	4.678E-11
2.0	2.771E-09	6.1	4.202E-11
2.1	2.434E-09	6.2	3.833E-11
2.2	2.137E-09	6.3	3.534E-11
2.3	1.876E-09	6.4	3.254E-11
2.4	1.644E-09	6.5	2.951E-11
2.5	1.440E-09	6.6	2.607E-11
2.6	1.262E-09	6.7	2.241E-11
2.7	1.103E-09	6.8	1.870E-11
2.8	9.638E-10	6.9	1.522E-11
2.9	8.417E-10	7.0	1.211E-11
3.0	7.345E-10	7.1	9.431E-12
3.1	6.402E-10	7.2	7.230E-12
3.2	5.581E-10	7.3	5.479E-12
3.3	4.859E-10	7.4	4.103E-12
3.4	4.229E-10	7.5	3.052E-12
3.5	3.676E-10	7.6	2.252E-12
3.6	3.193E-10	7.7	1.657E-12
3.7	2.775E-10	7.8	1.215E-12
3.8	2.406E-10	7.9	8.603E-13
3.9	2.100E-10	8.0	6.247E-13
4.0	1.841E-10	8.1	4.528E-13
4.1	1.624E-10	8.2	3.256E-13
4.2	1.459E-10	8.3	2.352E-13
4.3	1.322E-10	8.4	1.697E-13
4.4	1.214E-10	8.5	1.224E-13
4.5	1.132E-10	8.6	8.834E-14
4.6	1.069E-10	8.7	6.374E-14
4.7	1.019E-10	8.8	4.602E-14
4.8	9.686E-11	8.9	3.324E-14
4.9	9.169E-11	9.0	2.404E-14
5.0	8.627E-11		

show prominent presence in the high energy region resulting in formation of DR-bump in the recombination rates at high temperature where Ca XV can exist in stellar plasmas. These results should provide a more precise and complete modeling of astrophysical and laboratory applications, such as determination of Ca abundance.

The present cross sections are expected to be of accuracy of about 10%–15% for most of the energy and temperature region. Nahar (2017) obtained energies of Ca XV using this 29-CC wavefunction expansion and found agreement with observed energies within 1.5%. The present accuracy of σ_{PI} is estimated based on (i) good agreement of energies with the measured values, (ii) inclusion of a large number of core excitations, (iii) use of higher resolution for resonances, and (iv) consideration of large number configurations, and (v) the typical accuracy of R-matrix method and close coupling approximation.

The present 29-CC wavefunction includes core ion excitations going up to $n = 3$ in the high energy region where the ion can exist. The results are expected to be complete since the diminishing exponential factor of the recombination rate integral will converge faster at higher temperature. It is computationally prohibitive to check the convergence of contributions from even higher excitations in terms of numerical issues, computational time, and the practical need. As mentioned above, resonances due to $\Delta n > 1$ transitions from the ground state are much weaker and show convergence, a trend that been shown earlier by the author (e.g. Nahar and Pradhan (2016)).

The next step can be relativistic approximation for which extensive computations will involve 60 fine structure levels corresponding to the 29-LS states. With relativistic effects, additional resonances are expected to form by channels that are allowed in fine structure but not in LS coupling (e.g. Nahar (1998)). This will improve the accuracy of the recombination rates at low temperature plasmas. There will be more resonances as the core ion excitations in LS coupling will split in to a larger number of fine structure levels giving rise to more series of resonances. However, the recombination rate may not be affected much by the larger number of resonances as their contributions will be damped by the exponential factor of the recombination integral.

All photoionization and electron-ion recombination data are available electronically from on-line NORAD-Atomic-Data (NaharOSURadiativeAtomicData) webpage at <http://norad.astronomy.ohio-state.edu/>

Declaration of competing interest

The authors declare that they have no known competing financial interests or personal relationships that could have appeared to influence the work reported in this paper.

Acknowledgments

The computational work was carried out at the Ohio Supercomputer Center (OSC) in Columbus Ohio.

References

- Altun, Z., Yumak, A., Badnell, N.R., Colgan, J., Pindzola, M.S., 2004. *Astron. Astrophys.* 420, 775–781.
- Bell, R.H., Seaton, M.J., 1985. *J. Phys. B* 18, 1589–1629.
- Berrington, K.A., Burke, P.G., Butler, K., Seaton, M.J., Storey, P.J., Taylor, L.T., Yu, Y., 1987. *J. Phys. B* 20, 6379–6397.
- Berrington, K.A., Eissner, W., Norrington, P.H., 1995. *Comput. Phys. Commun.* 92, 290–420.
- Bhatia, A.K., Mason, H.E., 1986. *Astron. Astrophys.* 155, 417–419.
- Burke, P.G., Robb, W.D., 1975. *Adv. At. Mol. Phys.* 11, 143–214.
- Dere, K.P., 1978. *Astrophys. J.* 221, 1062–1067.
- Eissner, W., Jones, H., 1974. *Comput. Phys. Commun.* 8, 270–306.
- Gu, M.F., 2003. *Astrophys. J.* 590, 1131–1140.
- Hummer, D.G., Berrington, K.A., Eissner, W., Pradhan, A.K., Saraph, H.E., Tully, J.A., 1993. *Astron. Astrophys.* 279, 298–309.
- Jacobs, V.L., Davis, J., Rogerson, J.E., Blaha, M., Cainand, J., Davis, M., 1980. *Astrophys. J.* 239, 1119–1130.
- Laming, J.M., Drake, J.J., 1999. *Astrophys. J.* 516, 324–334.
- Luo, D., Pradhan, A.K., 1989. *J. Phys. B* 22, 3377–3395.
- Nahar, S.N., 1995. *Astrophys. J. Suppl.* 101 (423).
- Nahar, S.N., 1996. *Phys. Rev. A* 53 (2417).
- Nahar, S.N., 1998. *Phys. Rev. A* 58 (3766).
- Nahar, S.N., 2017. *New Astron.* 51, 69–73.
- Nahar, S.N., Eissner, W., Chen, G.X., Pradhan, A.K., 2003. *Astron. Astrophys.* 408, 789–801.
- Nahar, S.N., Pradhan, A.K., 1991. *Phys. Rev. A* 44 (2935).
- Nahar, S.N., Pradhan, A.K., 1992a. *Phys. Rev. A* 45, 7887–7893.
- Nahar, S.N., Pradhan, A.K., 1992b. *Phys. Rev. Lett.* 68 (1488).
- Nahar, S.N., Pradhan, A.K., 1994. *Phys. Rev. A* 49 (1816).
- Nahar, S.N., Pradhan, A.K., 2016. *Phys. Rev. Lett.* 116, 235003.
- Nahar, S.N., Pradhan, A.K., Zhang, H.L., 2000. *Astrophys. J. Suppl.* 131 (375).
- Pradhan, A.K., Nahar, S.N., 2011. *Atomic Astrophysics and Spectroscopy*. Cambridge University Press.
- Scott, N.S., Burke, P.G., 1980. *J. Phys. B* 12 (4299).
- Scott, N.S., Taylor, K.T., 1982. *Comput. Phys. Commun.* 25 (347).
- Seaton, M.J., 1987. *J. Phys. B* 20, 6363–6378.
- Shull, J.M.J.M., Van Steenberg, M., 1982. *Ap. J. Suppl. Ser.* 48, 95–107.
- The Opacity Project Team, 1995. *The Opacity Project*, Vol 1. Institute of Physics Publishing, p. 2, 1996.
- Yu, Y., Seaton, M.J., 1987. *J. Phys. B* 20, 6409–6429.